

Optimizing Unlicensed Band Spectrum Sharing With Subspace-Based Pareto Tracing

Zachary J. Grey[†], Susanna Mosleh[‡], Jacob D. Rezac[‡], Yao Ma[‡], Jason B. Coder[‡], and Andrew M. Dienstfrey[†]

[†]Information Technology Laboratory, Applied and Computational Mathematics Division, National Institute of Standards and Technology, USA

[‡]Communications Technology Laboratory, National Institute of Standards and Technology, USA

Abstract—In order to meet the ever-growing demands of data throughput for forthcoming and deployed wireless networks, new wireless technologies like Long-Term Evolution License-Assisted Access (LTE-LAA) operate in shared and unlicensed bands. However, the LAA network must co-exist with incumbent IEEE 802.11 Wi-Fi systems. We consider a coexistence scenario where multiple LAA and Wi-Fi links share an unlicensed band. We aim to improve this coexistence by maximizing the key performance indicators (KPIs) of these networks simultaneously via dimension reduction and multi-criteria optimization. These KPIs are network throughputs as a function of medium access control protocols and physical layer parameters. We perform an exploratory analysis of coexistence behavior by approximating active subspaces to identify low-dimensional structure of the optimization criteria, i.e., few linear combinations of parameters for simultaneously maximizing LAA throughput and Wi-Fi throughput. We take advantage of an aggregate low-dimensional subspace parametrized by approximated active subspaces of both throughputs to facilitate multi-criteria optimization. The low-dimensional subspace approximations enable visualizations suggesting a predominantly convex set of KPIs over active coordinates leading to an analytic Pareto trace of near-optimal solutions.

Index Terms—LTE-LAA, Wi-Fi, wireless coexistence, MAC and physical layer parameters, active subspace, Pareto trace

I. INTRODUCTION

As wireless communications evolve and proliferate into our daily lives, the demand for spectrum grows dramatically. To accommodate this growth, wireless device protocols are beginning to transition from a predominantly-licensed spectrum to a shared approach in which use of the unlicensed spectrum bands appears to be inevitable. The main bottleneck of this approach, however, is balancing new network paradigms with incumbent networks, such as Wi-Fi.

In order to deal with the spectrum scarcity, providers are beginning to operate Long-Term Evolution License-Assisted Access (LAA) in unlicensed bands. Even though operating LAA in unlicensed bands improves spectral-usage efficiency, it may have an enormous influence on Wi-Fi operation and create a number of challenges for both Wi-Fi and LTE networks as a means of constructively sharing the spectrum. Understanding and addressing these challenges calls for a deep dive into the operations and parameter selection of both networks in the medium access control (MAC) and physical layers.

There have been many investigations of fairness in spectrum sharing among LAA and Wi-Fi networks [1]–[3]—although,

these works do not consider optimizing key performance indicators (KPIs). Contrary to [1]–[3], the authors in [4] and [5] maximize LAA throughput and total network sum rate, respectively, over contention window sizes of both networks while guaranteeing the Wi-Fi throughput satisfies a threshold. However [4] and [5] optimize only a single MAC layer parameter. A multi-criteria optimization problem was formulated in [6] to satisfy the quality of service requirements of LAA eNodeBs by investigating the trade-off between the co-channel interference in the licensed band and the Wi-Fi collision probability in the unlicensed band. However, maximizing the Wi-Fi throughput was omitted. Considering both physical and MAC layer parameters, [7] maximizes the weighted sum rate of an LAA network subject to Wi-Fi throughput constraint with respect to the fraction of time that LAA is active. Alternatively, advantageous sharing of spectrum can be modeled as a multi-criteria optimization problem where both Wi-Fi and LAA KPIs, such as network throughputs on the unlicensed bands, are simultaneously maximized with respect to their physical and MAC layer parameters. The set of maximizing arguments quantify the inherent trade-off between LAA and Wi-Fi throughputs.

The multi-criteria optimization formalism we propose is further complicated by the high-dimensionality of the input space. Specifically, our model requires 17 MAC and physical layers variables to characterize the coexistence performance. Nevertheless, previous experience suggests that not all of these variables are equally important in determining KPIs quality. Active subspaces supplement an exploratory approach for determining parameter combinations which change KPI values the most, on average. The sets of parameter combinations defined by the active subspaces help inform KPI approximations and visualizations over an aggregate low-dimension subspace—simplifying the multi-criteria optimization.

We incorporate active subspace dimension reduction into a multi-criteria optimization framework to analyze the shared spectrum coexistence problem. The dimension reduction supplements a trade-off analysis of network throughputs by computing a Pareto trace. The Pareto trace provides a *continuous* approximation of Pareto optimal (non-dominated) points in a common domain of a multi-criteria problem [8], [9]—resulting in a near-best trade-off between differing throughputs. This offers a continuous description of a parameter subset which quantifies high quality performance of both networks, facilitated by a dimension reduction.

II. SYSTEM MODEL AND ASSUMPTIONS

We consider a downlink coexistence scenario where two mobile network operators (MNOs) operate over the same shared unlicensed industrial, scientific, and medical radio band. Previously, unlicensed bands were dominated by Wi-Fi traffic and, occasionally, used by commercial cellular carriers for offloading data otherwise communicated via LTE in the licensed spectrum. Lately, LTE carriers are choosing to operate in unlicensed bands in addition to data offloading. We assume the MNOs use time sharing to simultaneously operate in this band and we aim to analyze competing trade-offs in throughputs of the Wi-Fi and LTE systems. A network throughput is a function of both physical and MAC layer parameters. We introduce the parameters defining the network topology, the physical layer, MAC layer protocols, and briefly discuss the relation of these variables to network throughput.

We consider a coexistence scenario in which the LAA network consists of n_L eNodeBs, while the Wi-Fi network is composed of n_W access points (APs)¹. The eNodeBs and APs are randomly distributed over a particular area, while LAA user equipment (UEs) and Wi-Fi clients/stations (STAs) are uniformly and independently distributed around each eNodeB and AP, respectively. Each transmission node serves a set of single antenna UEs/STAs and the user association is based on the received power. We assume (i) both Wi-Fi and LAA are in the saturated traffic condition, i.e., at least one packet is waiting to be sent, (ii) there are neither hidden nodes nor false alarm/miss detection problems in the network², and (iii) the channel knowledge is ideal, so, the only source of unsuccessful transmission is collision. The physical data rate of the LAA and Wi-Fi networks is a function of signal-to-interference-plus-noise ratio (SINR) that is related to and changes with the link distances and propagation model. Any changes in data rates lead to different network throughput.

The medium access key feature in both Wi-Fi and LAA involves the station accessing the medium to sense the channel by performing clear channel assessment prior to transmitting. The station only transmits if the medium is determined to be idle. Otherwise, the transmitting station refrains from transmitting data until it senses the channel is available. Although LAA and Wi-Fi technologies follow similar channel access procedures, they utilize different carrier sense schemes, different channel sensing threshold levels, and different channel contention parameters, leading to different unlicensed channel access probabilities and thus, different throughputs.

Conforming with the analytical model in [7], [10], [11], the LAA and Wi-Fi throughputs, indicated respectively by $S_{\mathcal{L}}$ and

¹We are primarily focused on the operation of cellular base stations in the unlicensed bands. However, LTE base stations may have permission to utilize a licensed band as well. Moreover, our proposed subspace-based Pareto tracing approach could be applied to many types of communication systems, but LTE is used here as an example.

²We assume perfect spectrum sensing in both systems. The impact of imperfect sensing is beyond the scope of this paper and investigating the effect of sensing errors is an important topic for future work.

$S_{\mathcal{W}}$, are functions of m MAC and physical layer parameters in a vector θ conditioned on fixed values in a vector x ,

$$\begin{aligned} S_{\mathcal{L}} : \mathbb{R}^m \times \{x\} \rightarrow \mathbb{R} : (\theta, x) \mapsto S_{\mathcal{L}}(\theta; x), \\ S_{\mathcal{W}} : \mathbb{R}^m \times \{x\} \rightarrow \mathbb{R} : (\theta, x) \mapsto S_{\mathcal{W}}(\theta; x). \end{aligned} \quad (1)$$

For this application, LAA throughput $S_{\mathcal{L}}$ and Wi-Fi throughput $S_{\mathcal{W}}$ are only considered functions of m variable parameters in θ . This numerical study considers $m = 17$ parameters summarized in Table I. To simplify this study, we fix the remaining parameters in x governing the majority of the physical characteristics of the communication network—constituting a fixed *scenario* x for a parameter study over θ 's.

The problem of interest is to maximize a convex combination of network throughputs for the fixed scenario x over the MAC and physical layers parameters θ in a multi-criteria optimization. Mathematically, we define the *Pareto front* by the following optimization problem:

$$\underset{\theta \in \mathcal{D} \subset \mathbb{R}^m}{\text{maximize}} \quad tS_{\mathcal{L}}(\theta; x) + (1-t)S_{\mathcal{W}}(\theta; x), \quad (2)$$

for all $t \in [0, 1]$ where \mathcal{D} is the parameter domain defined by the ranges in Table I. The goal is to quantify a smooth trajectory $\theta(t)$ through MAC and PHY parameter space, or *trace* [9], such that the convex combination of throughputs is maximized over a map $\theta : [0, 1] \rightarrow \mathcal{D}$. In Section III, we summarize an exploratory approach for understanding to what extent problem (2) is convex [8]. The empirical evidence generated through visualization and dimension reduction provide justification for convex quadratic approximations and subsequent quadratic trace in Section IV.

III. ACTIVE SUBSPACES

Following the development in [12], we introduce an exploratory method for simplifying the problem statement in (2). For ease of exposition, in this section we denote either scalar-valued throughput function by $S : \mathcal{D} \subset \mathbb{R}^m \rightarrow \mathbb{R}$ with compact domain \mathcal{D} and assume all integrals and derivatives used in this discussion exist as measurable functions. The main results of the section rely on an eigendecomposition of the symmetric positive semi-definite matrix $C \in \mathbb{R}^{m \times m}$ defined as

$$C = \int_{\mathcal{D}} \nabla S(\theta) \nabla S(\theta)^T d\theta \quad (3)$$

with entries $C_{ij} = \int_{\mathcal{D}} (\partial S / \partial \theta_i) |_{\theta} (\partial S / \partial \theta_j) |_{\theta} d\theta$ for $i, j = 1, \dots, m$. For this application, the integral is taken uniformly over \mathcal{D} . The compact domain \mathcal{D} is a hyper-rectangle constructed³ from the Cartesian product of lower and upper bounds, $\theta_{i,\ell} \leq \theta_i \leq \theta_{i,u}$ for all $i = 1, \dots, m$.

If $\text{rank}(C) = r < m$, its eigendecomposition $C = W \Lambda W^T$ with orthogonal W satisfies $\Lambda = \text{diag}(\lambda_1, \dots, \lambda_m)$ with

$$\lambda_1 \geq \lambda_2 \geq \dots \geq \lambda_r > \lambda_{r+1} = \dots = \lambda_m = 0. \quad (4)$$

³The chosen definition of (3) weights all parameter combinations equally over \mathcal{D} and restricts the integration to feasible values (as summarized in Table I). Alternative choices are available in scenarios where it is more appropriate to weight parameters differently, but uniform is suitable to our application.

TABLE I: MAC and PHY parameters influencing throughputs

Parameters	Description	Bounds	Nominal	Parameters	Description	Bounds	Nominal
θ_1	Wi-Fi min contention window size	(8, 1024)	516	θ_{12}	α_{LoS}^*	(17.3, 21.5)	19.4
θ_2	LAA min contention window size	(8, 1024)	516	θ_{13}	α_{NLoS}^*	(31.9, 38.3)	35.1
θ_3	Wi-Fi max back-off stage	(10^{-4} , 8)	4	θ_{14}	Antenna gain at each transmitter	(10^{-4} dB, 5 dB)	2.5 dB
θ_4	LAA max back-off stage	(10^{-4} , 8)	4	θ_{15}	Noise figure at each receiver	(5 dB, 9 dB)	7 dB
θ_5	Distance between transmitters	(10 m, 20 m)	15 m	θ_{16}	Transmit power at each LAA eNodeB and Wi-Fi AP	(18 dBm, 23 dBm)	20.5 dBm
θ_6	Minimum distance between transmitters and receivers	(10m, 35 m)	22.5 m	θ_{17}	Carrier channel bandwidth	(10 MHz, 20 MHz)	15 MHz
θ_7	Height of each LAA eNodeB and Wi-Fi AP	(3 m, 6 m)	4.5 m	x_1	Number of LAA eNodeBs (n_L)	—	6
θ_8	Height of each LAA UEs and Wi-Fi STAs	(1 m, 1.5 m)	1.25 m	x_2	Number of Wi-Fi APs (n_W)	—	6
θ_9	Standard deviation of shadow fading	(8.03, 8.29)	8.16	x_3	Number of LAA UEs	—	6
θ_{10}	k_{LoS}^*	(45.12, 46.38)	45.75	x_4	Number of Wi-Fi STAs	—	6
θ_{11}	k_{NLoS}^*	(34.70, 46.38)	40.54	x_5	Number of unlicensed channels	—	1
				x_8	Scenario width	—	120 m
				x_9	Scenario height	—	80 m

Note: parameter ranges are established by 3GPP TS 36.213 V15.6.0 and 3GPP TR. 36.889 v13.0.0.

*The path-loss for both line-of-sight (LoS) and non-LoS scenarios can be computed as $k + \alpha \log_{10}(d)$ in dB, where d is the distance in meters between the transmitter and the receiver.

This defines two sets of important $\mathbf{W}_r = [\mathbf{w}_1 \dots \mathbf{w}_r] \in \mathbb{R}^{m \times r}$ and unimportant $\mathbf{W}_r^\perp = [\mathbf{w}_{r+1} \dots \mathbf{w}_m] \in \mathbb{R}^{m \times (m-r)}$ directions over the domain. The column span of \mathbf{W}_r and \mathbf{W}_r^\perp constitute the *active* and *inactive* subspaces, respectively. Note that (3) depends on a single scalar-valued response and potentially differs for the separate throughputs in (1).

What do we mean by *important directions*? Partitioning \mathbf{W} into m orthonormal eigenvectors $\mathbf{w}_i \in \mathbb{R}^m$ representing the columns, $\mathbf{W} = [\mathbf{w}_1 \dots \mathbf{w}_m]$, we can simplify $\mathbf{w}_i^T \mathbf{C} \mathbf{w}_i$ to obtain an expression for the eigenvalues,

$$\lambda_i = \int_{\mathcal{D}} (\mathbf{w}_i^T \nabla S(\boldsymbol{\theta}))^2 d\boldsymbol{\theta}. \quad (5)$$

Reinterpreting the integral by definition of the expectation, $\mathbb{E}[f(\boldsymbol{\theta})] = \int_{\mathcal{D}} f(\boldsymbol{\theta}) d\boldsymbol{\theta}$ for any measurable f , the eigenvalues can be interpreted as the mean squared directional derivative of S in the direction of $\mathbf{w}_i \in \mathbb{R}^m$. Precisely, the directional derivative can be written $dS_{\boldsymbol{\theta}}[\mathbf{w}] = \mathbf{w}^T \nabla S(\boldsymbol{\theta})$ and we obtain $\lambda_i = \mathbb{E}[dS_{\boldsymbol{\theta}}^2[\mathbf{w}_i]]$ —the i^{th} eigenvalue is the mean squared directional derivative in the direction of the i^{th} eigenvector. Thus, the inherent ordering (4) of the eigenpairs $\{(\lambda_i, \mathbf{w}_i)\}_{i=1}^m$ indicate directions \mathbf{w}_i which change the function S the most, on average, up to the $r+1, \dots, m$ directions which *do not change the function at all*. In other words, the directional derivatives over the inactive subspace, $\text{Range}(\mathbf{W}_r^\perp)$, are zero provided the corresponding eigenvalues are zero. In fact, either throughput response from (1) is referred to as a *ridge function* over $\boldsymbol{\theta}$'s if and only if $dS_{\boldsymbol{\theta}}[\mathbf{w}] = 0$ for all $\mathbf{w} \in \text{Null}(\mathbf{W}_r^\perp)$.

Naturally, if the trailing eigenvalues are merely small as opposed to identically zero, then the function changes much less over the inactive directions which have smaller directional derivatives. This lends itself to a framework for reduced-dimension approximation of the function such that we only approximate changes in the function over the first r active directions and take the approximation to be constant over the trailing $m-r$ inactive directions [12]. Such an approximation to S is called a *ridge approximation* by a function H referred to as the *ridge profile*, i.e.,

$$S(\boldsymbol{\theta}) \approx H(\mathbf{W}_r^T \boldsymbol{\theta}). \quad (6)$$

In the event that the trailing eigenvalues of \mathbf{C} are zero, then the approximation is exact for a particular H [12].

In either case, approximation or an exact ridge profile, the possibility of reducing dimension by projection to fewer, $r < m$, *active coordinates* $\mathbf{y} = \mathbf{W}_r^T \boldsymbol{\theta} \in \mathbb{R}^r$ can enable higher-order polynomial approximations for a given data set of coordinate-output pairs and an ability to *visualize* the approximation. For example, we can visualize the approximation by projection to the active coordinates when r is chosen to be 1 or 2 based on the decay and gaps in the eigenvalues. These subsequent visualizations are referred to as *shadow plots* [13] or graphs $\{(\mathbf{W}_r^T \boldsymbol{\theta}_i, S(\boldsymbol{\theta}_i)\}_{i=1}^N$ for N samples $\boldsymbol{\theta}_i$ drawn uniformly (for this application). A strong decay leading to a small sum of trailing eigenvalues implies an improved approximation over relatively few important directions while larger gaps in eigenvalues imply an improved approximation to the low-dimensional subspace [12]. Identifying if this structure exists depends on the decay and gaps in eigenvalues. We can subsequently exploit any reduced dimensional visualization and approximation to simplify our problem (2). However, we must reconcile that our problem of interest involves two separate computations of throughput, $S_{\mathcal{L}}$ and $S_{\mathcal{W}}$.

Independently approximating active subspaces for the objectives $S_{\mathcal{L}}$ and $S_{\mathcal{W}}$ generally results in different subspaces of the shared parameter domain. The next challenge is to define a common subspace that, while sub-optimal for each objective, is nevertheless sufficient to capture the variability of both simultaneously. Assume that we can reduce important parameter combinations to a common dimension r of potentially distinct subspaces. These subspaces are spanned by the column spaces of $\mathbf{W}_{r,\mathcal{L}}$ and $\mathbf{W}_{r,\mathcal{W}}$ chosen as the first r eigenvectors resulting from separate approximations of (3) for LAA and Wi-Fi throughputs, respectively. The challenge is to appropriately “mix” the subspaces so we may formulate a solution to (2) over a common dimension reduction.

One method to find an appropriate subspace mix is to take the union of both subspaces. However, if $r \geq 2$ and $\text{Range}(\mathbf{W}_{r,\mathcal{L}}) \cap \text{Range}(\mathbf{W}_{r,\mathcal{W}}) = \{\mathbf{0}\}$ then the com-

bined subspace dimension is inflated and visualization of subsequent convex approximations becomes challenging. We use interpolation between the two subspaces to overcome these difficulties and retain the common reduction to an r -dimensional subspace. The space of all r -dimensional subspaces in \mathbb{R}^m is the $r(m-r)$ -dimension Grassmann manifold (Grassmannian⁴) denoted $\text{Gr}(r, m)$ [14]. Utilizing the analytic form of a geodesic over the Grassmannian [14], we can smoothly interpolate from one subspace to another—an interpolation which is, in general, non-linear. This is particularly useful because the *distance* between any two subspaces along such a path, $[\mathbf{U}_r] : \mathbb{R} \rightarrow \text{Gr}(r, m) : s \mapsto [\mathbf{U}_r(s)]$ for all $s \in [0, 1]$, minimizes the distance between the two subspaces $\text{Range}(\mathbf{W}_{r,\mathcal{L}}), \text{Range}(\mathbf{W}_{r,\mathcal{W}}) \in \text{Gr}(r, m)$ defining the geodesic. That is, the geodesic $[\mathbf{U}_r(s)]$ minimizes the distance between $\text{Range}(\mathbf{W}_{r,\mathcal{L}})$ and $\text{Range}(\mathbf{W}_{r,\mathcal{W}})$ while still constituting an r -dimensional subspace in \mathbb{R}^m .

After approximating $\mathbf{W}_{r,\mathcal{L}}$ and $\mathbf{W}_{r,\mathcal{W}}$ we must make an informed decision to take the union of subspaces or compute a new subspace $\text{Range}(\mathbf{U}_r)$ against some criteria parametrized over the Grassmannian geodesic. Then we may restate the original problem with a common dimension reduction, $\mathbf{y} = \mathbf{U}_r^T \boldsymbol{\theta}$, utilizing updated approximations over $r < m$ combined/mixed active coordinates,

$$\underset{\mathbf{y} \in \mathcal{Y}}{\text{maximize}} \quad tH_{\mathcal{L}}(\mathbf{y}; \mathbf{x}) + (1-t)H_{\mathcal{W}}(\mathbf{y}; \mathbf{x}), \quad (7)$$

for all $t \in [0, 1]$. Once again, this optimization problem involves a closed and bounded feasible domain of parameter values $\mathcal{Y} = \{\mathbf{y} \in \mathbb{R}^r : \mathbf{y} = \mathbf{U}_r^T \boldsymbol{\theta}, \boldsymbol{\theta} \in \mathcal{D}\}$ which remains convex for convex \mathcal{D} and a new subspace $\text{Range}(\mathbf{U}_r)$. The utility of the dimension reduction is the ability to formulate a continuous *trace* of the Pareto front [9]—involving the inverse of a convex combination of Hessians—in fewer dimensions. This is supplemented by visualization in the case $r = 1$ or $r = 2$ providing *empirical evidence of convexity*. The convex approximations and visualizations are summarized in Section IV.

A. Computational Considerations

In order to approximate the eigenspaces of $\mathbf{C}_{\mathcal{L}}$ and $\mathbf{C}_{\mathcal{W}}$ for the separate responses (1) we must first approximate the gradients of the network throughput responses which are not available in an analytic form. Specifically, we use forward finite difference approximations to approximate the partial derivatives in (3). These computations are supplemented by a rescaling of all parameters to a unit-less domain which permits consistent finite-difference step sizes.

The rescaling transformation is chosen based on the provided upper and lower bounds, summarized in Table I. This ensures that the scale of any one parameter does not influence finite difference approximations. Moreover, this alleviates the

⁴Formally, an element of the Grassmannian is an equivalence class, $[\mathbf{U}_r]$, of all orthogonal matrices whose first r columns span the same subspace as $\mathbf{U}_r \in \mathbb{R}^{m \times r}$. That is, the equivalence relation $X \sim Y$ is given by $\text{Range}(X) = \text{Range}(Y)$ denoted $[X]$ or $[Y]$ for $X, Y \in \mathbb{R}^{m \times r}$ with orthonormal columns.

need for an interpretation or justification when taking linear combinations of parameters with differing units. Because the throughput calculations involve parameter combinations appearing as exponents in the composition of a variety of computations, we use a uniform sampling of log-scaled parameter values. This transforms parameters appearing as exponents to appear as coefficients—a useful transformation given that we ultimately seek an approximation of linear combinations of parameters inherent to the definition of a subspace.

The resulting scaling of the domain is achieved by the composition of transformations $\tilde{\boldsymbol{\theta}} = \mathbf{M} \ln(\boldsymbol{\theta}) + \mathbf{b}$ where $\mathbf{M} = \text{diag}(2/(\ln(\theta_{u,1}) - \ln(\theta_{\ell,1})), \dots, 2/(\ln(\theta_{u,m}) - \ln(\theta_{\ell,m})))$, $\mathbf{b} = -\mathbf{M} \mathbb{E}[\ln(\boldsymbol{\theta})]$, and $\ln(\cdot)$ is taken component-wise. To compute this transformation, we take $\theta_{\ell,i}$ and $\theta_{u,i}$ as the i -th entries of the lower and upper bounds and $\mathbb{E}[\ln(\boldsymbol{\theta})]$ the mean of $\ln(\boldsymbol{\theta}) \sim U_m[\ln(\boldsymbol{\theta}_{\ell}), \ln(\boldsymbol{\theta}_u)]$. This particular choice of scaling ensures $\tilde{\boldsymbol{\theta}} \in [-1, 1]^m$ and $\mathbb{E}[\tilde{\boldsymbol{\theta}}] = \mathbf{0}$ so the resulting domain is also centered. Lastly, we use Monte Carlo as a constant coefficient quadrature rule to approximate the integral form of the two separate matrices, defined by (3), for the two throughputs. The details are provided as Algorithm 1.

The selection of r in Algorithm 1 can be automated by, for example, a heuristic which takes the largest gap in eigenvalues [12]. For simplicity, we take an exploratory approach to sele-

Algorithm 1 Monte Carlo Approximation of Throughput Active Subspaces using Forward Differences

Require: Forward maps $S_{\mathcal{L}}$ and $S_{\mathcal{W}}$, small coordinate perturbation $h \geq 0$, fixed scenario parameters \mathbf{x} , and parameter bounds $\boldsymbol{\theta}_{\ell}, \boldsymbol{\theta}_u \in \mathbb{R}^m$.
1: Generate N random samples uniformly, $\{\tilde{\boldsymbol{\theta}}_i\}_{i=1}^N \sim U_m[-1, 1]$.
2: Compute \mathbf{M} , \mathbf{M}^{-1} , and \mathbf{b} according to a uniform distribution of log-scale parameters given $\boldsymbol{\theta}_{\ell}$ and $\boldsymbol{\theta}_u$.
3: **for** $i = 1$ to N **do**
4: Transform the uniform log-scale sample to the original scale $\boldsymbol{\theta}_i = \exp(\mathbf{M}^{-1}(\tilde{\boldsymbol{\theta}}_i - \mathbf{b}))$ where the exponential is taken component-wise.
5: Evaluate forward maps $(S_{\mathcal{L}})_i = S_{\mathcal{L}}(\boldsymbol{\theta}_i; \mathbf{x})$ and $(S_{\mathcal{W}})_i = S_{\mathcal{W}}(\boldsymbol{\theta}_i; \mathbf{x})$.
6: **for** $j = 1$ to m **do**
7: Transform the j -th coordinate perturbation to the original input scale $\boldsymbol{\theta}_h = \exp(\mathbf{M}^{-1}(\tilde{\boldsymbol{\theta}}_i + h \mathbf{e}_j - \mathbf{b}))$.
8: Approximate the j -th entry of the gradient at the i -th sample as

$$(\tilde{\nabla} S_{\mathcal{L}})_{i,j} = \frac{S_{\mathcal{L}}(\boldsymbol{\theta}_h; \mathbf{x}) - (S_{\mathcal{L}})_i}{h},$$

similarly for $(\tilde{\nabla} S_{\mathcal{W}})_{i,j}$, where \mathbf{e}_j is the j -th column of the m by m identity matrix.

9: **end for**
10: **end for**
11: Take the average of the outer product of approximated gradients as

$$\tilde{\mathbf{C}}_{\mathcal{L}} = \frac{1}{N} \sum_{i=1}^N (\tilde{\nabla} S_{\mathcal{L}})_{i,:} \otimes (\tilde{\nabla} S_{\mathcal{L}})_{i,:},$$

similarly for $\tilde{\mathbf{C}}_{\mathcal{W}}$, where the tensor (outer) product is taken over the j -th index.

12: Approximate the eigenvalue decompositions

$$\tilde{\mathbf{C}}_{\mathcal{L}} = \tilde{\mathbf{W}}_{\mathcal{L}} \tilde{\boldsymbol{\Lambda}}_{\mathcal{L}} \tilde{\mathbf{W}}_{\mathcal{L}}^T \quad \text{and} \quad \tilde{\mathbf{C}}_{\mathcal{W}} = \tilde{\mathbf{W}}_{\mathcal{W}} \tilde{\boldsymbol{\Lambda}}_{\mathcal{W}} \tilde{\mathbf{W}}_{\mathcal{W}}^T$$

ordered by decreasing eigenvalues.

13: Observe the eigenvalue decay and associated gaps to inform a reasonable choice of r .

14: **return** The first r columns of $\tilde{\mathbf{W}}_{\mathcal{L}}$ and $\tilde{\mathbf{W}}_{\mathcal{W}}$, denoted $\tilde{\mathbf{W}}_{r,\mathcal{L}}$ and $\tilde{\mathbf{W}}_{r,\mathcal{W}}$.

acting r which requires some user-input. We seek a visualization of the response to provide empirical evidence that the throughputs are predominantly convex and hence require $r \leq 2$. We then check that the result offers acceptable approximations of throughputs with sufficient gaps in the second and third eigenvalues suggesting reasonable subspace approximations.

IV. SIMULATION AND RESULTS

We demonstrate the ideas proposed in Section III on the LAA-Wi-Fi coexistence scenario described in Section II to maximize both throughputs simultaneously. We apply active subspaces to simplify the multi-criteria optimization problem (2) by focusing on a reduced set of mixed MAC and physical layer parameter combinations informing a trace of near Pareto optimal solutions. Table I summarizes the scenario parameters and parameter bounds used to inform the throughput computations and domain scaling, respectively.

The numerical experiment utilizes $N = 1000$ samples resulting in $N(m+1) = 18,000$ function evaluations to compute forward differences with $h = 10^{-6}$. The resulting decay in eigenvalues gave relatively accurate degree-2 to degree-5 least-squares polynomial approximations—computed utilizing sets of coordinate-output pairs $\{(\tilde{\mathbf{W}}_{r,\mathcal{L}}^T \tilde{\boldsymbol{\theta}}_i, (S_{\mathcal{L}})_i)\}_{i=1}^N$ and $\{(\tilde{\mathbf{W}}_{r,\mathcal{W}}^T \tilde{\boldsymbol{\theta}}_i, (S_{\mathcal{W}})_i)\}_{i=1}^N$ —with varying coefficients of determination between 0.83–0.98 for both throughputs when $r = 1$ or $r = 2$. In an effort to improve the ridge approximation while retaining the ability to visualize the response for the quadratic polynomial, we fix $r = 2$ and mix the subspaces according to a quadratic approximation with corresponding coefficients of determination $R_{\mathcal{L}}^2$ and $R_{\mathcal{W}}^2$ —computed using new sets of subspace coordinates and throughput (coordinate-output) pairs. We select a criteria to mix subspaces achieving a balanced approximation when $r = 2$. This offers a subproblem,

$$\underset{s \in [0,1]}{\text{maximize}} \min\{R_{\mathcal{L}}^2(s), R_{\mathcal{W}}^2(s)\}, \quad (8)$$

where the separate throughput coefficients of determination, $R_{\mathcal{L}}^2(s)$ and $R_{\mathcal{W}}^2(s)$, are parametrized by successive quadratic fits over new coordinates $\mathbf{y}_i = \mathbf{U}_r^T(s)\tilde{\boldsymbol{\theta}}_i$ for all $i = 1, \dots, N$ defined by the Grassmannian geodesic $[\mathbf{U}_r(s)]$ beginning at $\text{Range}(\tilde{\mathbf{W}}_{r,\mathcal{W}})$ and ending at $\text{Range}(\tilde{\mathbf{W}}_{r,\mathcal{L}})$.

The univariate subproblem in (8) can be visualized and, in this experiment, achieved a unique maximizing argument $s^* \in [0,1]$ admitting a mixed subspace with orthonormal basis given by two columns in a matrix $\mathbf{U}_r(s^*) = [\mathbf{u}_1 \mathbf{u}_2]$, i.e., $[\mathbf{u}_1 \mathbf{u}_2] \in \mathbb{R}^{m \times 2}$ taken at the optimal s^* is the representative element of $[\mathbf{U}_r(s^*)]$. The coefficients of determination varied monotonically and intersected over the Grassmannian parametrization. Consequently, the subproblem results in an approximately equal criteria for the accuracy of the quadratic ridge profiles $H_{\mathcal{W}}$ and $H_{\mathcal{L}}$, i.e., $R_{\mathcal{L}}^2(s^*) \approx R_{\mathcal{W}}^2(s^*) \approx 0.90$. The choice of quadratic least-squares approximation over mixed active coordinates admits an analytic form [9] for the Pareto trace of (7). The analytic form of the quadratic trace is

taken as a convenience in contrast to a higher-order polynomial approximation—or alternative approximation—and subsequent trace. Part of the utility afforded by the dimension reduction is simultaneously fitting and visualizing higher-order approximations over the low-dimensional coordinates for the fixed sample size of coordinate-output pairs, N . However, the quadratic fits were deemed reasonable approximations admitting convexity which can be observed directly in the shadow plots. The convex quadratic ridge approximations, quadratic Pareto trace, and projected boundary of the domain over the mixed subspace are shown in Fig. 1. Additionally, the Pareto front approximation resulting from the quadratic trace is shown with the non-dominated designs in Fig. 2.

Observing Fig. 1, the continuous Pareto trace over the subspace coordinates (red curve) moves approximately through the collection of projected non-dominated designs (black circles). The non-dominated designs are determined from the $N = 1000$ random samples; sorted according to [15]. However, it is not immediately clear through this visualization that the non-dominated designs constitute elements of an alternative continuous approximation of the Pareto front—perhaps represented by an alternative low-dimensional manifold. Instead, we have supplemented a continuous parametrization of the Pareto front which is implicitly regularized as a solution over a low-dimension subspace. However, there are infinite $\boldsymbol{\theta}$ in the original parameter space which correspond to points along the trace depicted in Fig. 1—i.e., infinitely many $m - r$ inactive coordinate values which may change throughputs albeit significantly less than the two mixed active coordinates, $y_1 = \mathbf{u}_1^T \tilde{\boldsymbol{\theta}}$ and $y_2 = \mathbf{u}_2^T \tilde{\boldsymbol{\theta}}$. To reconcile the choice of infinitely many inactive coordinates, we visualize subsets of 25 inactive coordinate samples drawn randomly over $\text{Null}(\mathbf{U}_r^T(s^*))$ along a discretization of the trace. Fig. 2 depicts the corresponding throughput evaluations from the inactive samples as red dots along the approximated Pareto front—the red line connects conditional averages of throughputs over inactive samples along corresponding points over the trace. The visualization emphasizes that the throughputs change significantly less over the inactive coordinates in contrast to the range of values observed over the trace.

There is some bias in the approximation of the Pareto front (red curve) in Fig. 2 which is not a least-squares curve of non-dominated throughput values (black circles) potentially due in part to the quadratic ridge approximations. We expect refinements to these approximations will further improve the continuous Pareto approximation (shown in red in Fig. 2).

V. CONCLUSION & FUTURE WORK

We have proposed a technique to simultaneously optimize the performance of multiple MNOs sharing limited unlicensed spectrum resources. An exploratory analysis utilizing an example of LAA coexistence with Wi-Fi network identified a common subspace-based dimension reduction of a basic model of network behavior. This enabled visualizations and low-dimensional approximations which led to a *continuous* approximation of the Pareto frontier for the multi-criteria problem of

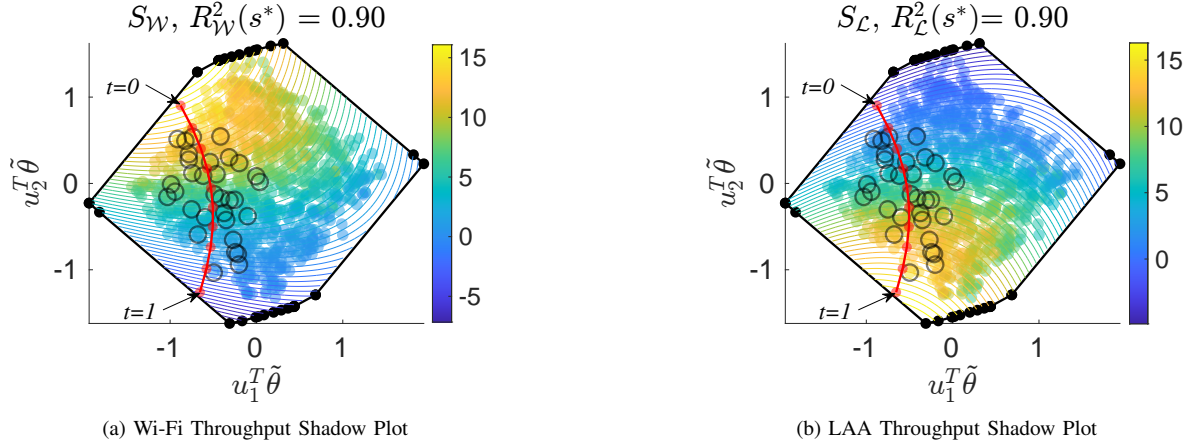


Fig. 1: Pareto trace of quadratic ridge profiles. The quadratic Pareto trace (red curve and dots) is overlaid on a shadow plot over the mixed coordinates (colored scatter) with the projected bounds and vertices of the domain (black dots and lines), \mathcal{Y} . The quadratic approximations (colored contours) are computed as least-squares fits over the mixed subspace coordinates. Also depicted is the projection of the non-dominated domain values from the $N = 1000$ random samples (black circles). The trace begins at $t = 0$ with near maximum quadratic Wi-Fi throughput and we move (smoothly) along the red curve to $t = 1$ obtaining near maximum quadratic LAA throughput—maintaining an approximately best trade-off over the entire curve restricted to \mathcal{Y} .

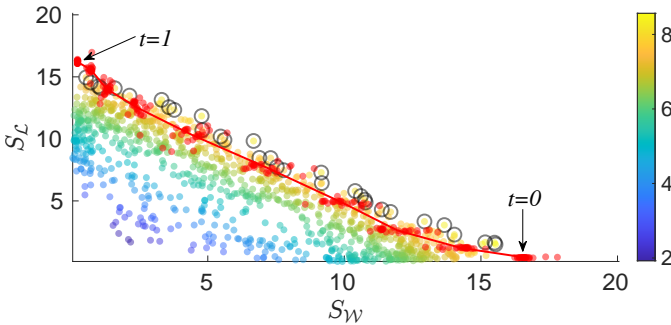


Fig. 2: Approximation of the Pareto front resulting from the quadratic trace. The approximate Pareto front (red curve) is shown with the non-dominated throughput values (black circles) and scatter of $N = 1000$ random responses colored according to the averaged throughputs. The red curve is the image of the continuous trace through parameter space (visualized as the red curve in Fig. 1) representing a near Pareto optimal set of solutions.

maximizing all convex combinations of network throughputs over MAC and PHY parameters. Such a result simplifies the search for parameters which enable high quality performance of both networks, particularly compared to approaches which do not operate on a reduced parameter space. Analysis of the LAA-Wi-Fi example revealed an explainable and interpretable solution to an otherwise challenging problem—*devoid of any known convexity until subsequent exploration*.

Future work will incorporate alternative low-dimensional approximations including both cases of Grassmannian mixing and subspace unions to improve the trace. We will also summarize a sensitivity analysis, active subspace approximation diagnostics, and the parametrization of a predominantly flat manifold of near Pareto optimal solutions. Future approaches will enable spectrum sharing in unlicensed bands by simplifying the design of wireless network operation and architecture—ultimately quantifying MAC and PHY parameter combinations giving near-optimal KPI trade-offs.

REFERENCES

- [1] H. He, H. Shan, A. Huang, L. Cai, and T. Quek, “Proportional Fairness Based Resource Allocation for LTE-U Coexisting With WiFi,” *IEEE Access*, vol. 5, pp. 4720–4731, Sept. 2016.
- [2] C. Cano, D. Leith, A. Garcia-Saavedra, and P. Serrano, “Fair Coexistence of Scheduled and Random Access Wireless Networks: Unlicensed LTE/WiFi,” *IEEE ACM Trans. Netw.*, vol. 25, no. 6, pp. 3267–3281, Dec. 2017.
- [3] M. Mehrnoush, S. Roy, V. Sathya, and M. Ghosh, “On the Fairness of Wi-Fi and LTE-LAA Coexistence,” *IEEE Trans. Cognitive Commun. and Netw.*, vol. 4, no. 4, pp. 735–748, Dec. 2018.
- [4] Y. Gao, B. Chen, C. Xiaoli, and J. Zhang, “Resource Allocation in LTE-LAA and WiFi Coexistence: a Joint Contention Window Optimization Scheme,” *IEEE Global Commun. Conf.*, Dec. 2017.
- [5] Y. Gao, “LTE-LAA and WiFi in 5G NR Unlicensed: Fairness, Optimization and Win-Win Solution,” *IEEE SmartWorld/SCALCOM/UIC/ATC/CBDCom/IOP/SCI*, Aug. 2019.
- [6] R. Yin, G. Yu, A. Maaref, and G. Y. Li, “A Framework for Co-Channel Interference and Collision Probability Tradeoff in LTE Licensed-Assisted Access Networks,” *IEEE Trans. Wireless Commun.*, vol. 15, no. 9, pp. 6078–6090, Sept. 2016.
- [7] S. Mosleh, Y. Ma, J. B. Coder, E. Perrins, and L. Liu, “Enhancing LAA co-existence using MIMO under imperfect sensing,” *IEEE Globecom Workshops*, pp. 1–6, Dec. 2019.
- [8] S. Boyd and L. Vandenberghe, *Convex optimization*. Cambridge university press, 2004.
- [9] M. Bolten, O. T. Doganay, H. Gottschalk, and K. Klamroth, “Tracing locally pareto optimal points by numerical integration,” *arXiv*, Apr. 2020. [Online]. Available: <https://arxiv.org/abs/2004.10820>
- [10] S. Mosleh, Y. Ma, J. D. Rezac, and J. B. Coder, “Dynamic spectrum access with reinforcement learning for unlicensed access in 5G and beyond,” *IEEE 91st Veh. Technol. Conf.*, May 2020.
- [11] —, “A novel machine learning approach to estimating KPI and PoC for LTE-LAA-based spectrum sharing,” *IEEE Int. Conf. on Commun. Workshops*, June 2020.
- [12] P. G. Constantine, *Active Subspaces: Emerging Ideas in Dimension Reduction for Parameter Studies*. SIAM-Society for Industrial and Applied Mathematics, Mar. 2015.
- [13] Z. J. Grey and P. G. Constantine, “Active subspaces of airfoil shape parameterizations,” *AIAA Journal*, vol. 56, no. 5, pp. 2003–2017, Apr. 2018.
- [14] A. Edelman, T. A. Arias, and S. T. Smith, “The geometry of algorithms with orthogonality constraints,” *SIAM J. Matrix Anal. Appl.*, vol. 20, no. 2, pp. 303–353, 1998.
- [15] H.-T. Kung, F. Luccio, and F. P. Preparata, “On finding the maxima of a set of vectors,” *Journal of the ACM (JACM)*, vol. 22, no. 4, pp. 469–476, 1975.